Title
Potential Composite Solid-State Electrolyte for Lithium-Ion Batteries

Author
Chu, Heng Jui

Publication Date
2023

Peer reviewed|Thesis/dissertation

UNIVERSITY OF CALIFORNIA

Los Angeles

Potential Composite Solid-State Electrolyte for Lithium-Ion Batteries

A thesis submitted with partial satisfaction

of the requirements for the degree Master of Science

in Materials Science and Engineering

by

Heng Jui Chu

2023

ABSTRACT OF THE THESIS

Potential Solid-state electrolyte for Lithium-ion batteries

by

Heng Jui Chu

Master of Science in Materials Science and Engineering

University of California, Los Angeles, 2023

Professor Ximin He, Chair

Lithium-ion batteries are usually used in power tools, electric vehicles, and portable electronics because of their high capacities, high voltages, and long lifetime. However, the conventional organic liquid electrolyte is highly flammable and there is a leakage risk. As a result, solid-state electrolytes are widely studied for next-generation batteries. Herein, an electrolyte with both high conductivity and mechanical strength is developed by using a composite electrolyte. The lithium lanthanum titanate (LLTO)/poly(ethylene oxide) electrolyte (PEO) with the addition of porous polyvinyl alcohol (PVA) as a polymer framework was used to increase mechanical strength.

The thesis of Heng Jui Chu is approved.

Yu Huang

Aaswath Pattabhi Raman

Ximin He, Committee Chair

University of California, Los Angeles

2023

Content

List of Figures

List of Tables

ACKNOWLEDGEMENTS

I would like to express my gratitude to Dr. He for her guidance and show my appreciation to members of the He Lab for their assistance.

I would also like to thank Dr. Yu Huang and Dr. Aaswath Raman for being on my committee and reviewing this work.

Lastly, I am grateful for the love and support that my family and friends have given me.

Chapter 1 Background

1.1 Introduction

Energy storage and environmental pollution have been serious problems since the industrial revolution. For example, with the widely used thermal power, the emission of CO_2 is unneglectable. We are enduring serious greenhouse effects. Scientists have been dedicated to developing more efficient energy conversion and renewable energy systems, including solar cells, fuel cells, and batteries. During the oil crisis, Stanley Whittingham brought up the idea of rechargeable batteries, which gave us the hope of a more convenient life with fossil-free energy [1]. He developed layered titanium disulfide as a cathode material with the intercalation mechanism of LIBs. Since then, rechargeable lithium-ion batteries have been significantly developed.

With the great performance of lithium-ion battery (LIB), it is usually used in power tools, electric vehicles, and portable electronics. It exhibits a high capacity, high voltage, long lifetime, and low self-discharge. LIB has a high capacity because of the smallest ionic radii of lithium among all the single-charged ions and the high voltage results from the lowest reduction potential of lithium metal [2]. The voltage of the battery could be up to 3.6 V for a carbon anode battery. Furthermore, there is no memory effect for the charge and discharge process. However, the safety issue is one of the concerns that hinders further development. Especially when electric vehicles are in increasing demand nowadays, the safety issue becomes more important. Fire

accidents could be caused by thermal runaway, dendrite growth, electrolyte leakage, or abused operations, which could be improved by the desired design of each battery component [3].

1.2 Mechanism and Component of Lithium-Ion Batteries

A battery is a system that converts chemical energy into electrical energy. It typically contains four components, cathode, anode, separator, and electrolyte. In the discharging process, lithium ions flow from the anode to the cathode through an electrolyte, and electrons move from the anode to the cathode through an external circuit, as shown in figure 1.1. The anode is the source of lithium ions and undergoes the oxide reaction. The electrolyte is the medium for ion transportation and the separator helps to prevent the contact between cathode and anode caused by dendrite growth. Since lithium ions move back and forth between the two electrodes, lithium-ion batteries are also known as rocking-chair batteries or swing batteries. Usually, commercial LIBs use layered lithium compound material as a cathode. Cathode materials include $LiCoO_2$ (LCO), $LiFePO_4$ (LFP), $LiMnO_2O_4$ (LMO), and $LiNiMnCoO_2$ (NMC). Graphite is usually used as an anode. Using LCO/graphite as an example, the discharge reactions of electrodes are shown as follows:

Cathode: $LiCoO_2 \rightarrow Li_{1-x}CoO_2 + Li^+ + xe^-$

Anode: $C + xLi^+ + xe^- \rightarrow Li_xC$

Overall reaction: $LiCoO_2 + C \rightarrow Li_{1-x}CoO_2 + Li_xC$

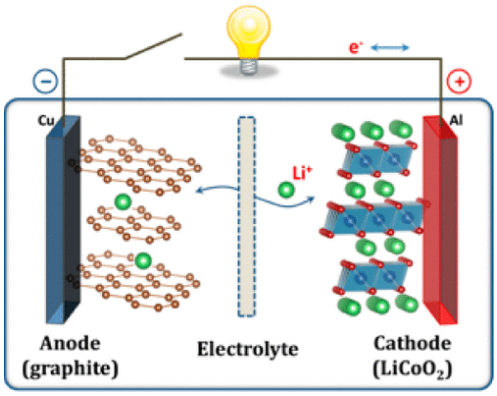

Figure 1.1 Illustration of the working mechanism of lithium-ion batteries [4].

1.3 Electrolyte

Current commercial LIB uses an organic liquid electrolyte, but nowadays scientists are devoted to developing solid-state batteries for their good stability and mechanical strength. There are some requirements for the electrolyte. First, it should be ionic conductive and, at the same time, be an electronic insulator to prevent self-discharge while having facile ion transportation. Second, it should have a wide electrochemical window to prevent electrolyte degradation of cathodes and anodes within the working potentials. Third, it should be inert to other cell components. Last, it should be robust against electrical, mechanical, or thermal abuses [5].

The conventional organic liquid electrolyte is typically composed of 1 M $LiPF_6$ salt, ethylene carbonate (EC)-based, and ethyl methyl carbonate (EMC) [5]. The liquid organic electrolyte has high conductivity and wettability on electrode surfaces. The ionic conductivity is about 10^{-3} to 10^{-2} S cm^{-1}. However, with the separator, the effective conductivity is about 10^{-4} S cm^{-1} [6]. Furthermore, the electrochemical property of organic liquid is unstable, and it is highly

flammable. Its flammability is caused by low flash point, which is below 30 °C [5]. During the charge/discharge process, electrodes will generate heat and then organic liquid electrolyte can behave as a fuel source [3][5]. If the heat dissipation is poor in the cell, the possibility of an explosion gets higher. As a result, solid-state electrolyte (SSE) is a promising candidate for next-generation batteries.

1.4 Solid-State Electrolyte

Solid-state electrolyte prevents dendrite growth, and shows higher thermal and electrochemical stabilities, allowing us to use lithium metal as an anode [7][8]. Lithium metal can increase by 50 % of energy density compared with graphite anode [9]. SSE can also serve as the separator, which makes fabrication easier. Usually, SSE is classified into three types: inorganic, polymer, and composite electrolyte.

1.4.1 Inorganic Solid Electrolyte

The first inorganic solid electrolyte (ISE), silver ionic compound Ag_3SI, was found in the 1960s. The conductivity is about 10^{-2} S/cm at room temperature. However, it is very brittle [10]. Now oxide-group and sulfide-group electrolytes are widely used [8]. Because the ceramic shows a high intrinsic bulk ionic conductivity, these materials are also known as superionic conductors. There are a lot of defects in the structure, so the active energy is low. Second, instead of a single ion, multiple ions hop at the same time. The strong ion-ion interactions lead to a lower barrier energy, as shown in figure 1.2 [11]. Third, because the sublattice is highly disordered, it’s easier for ions to hop between lattices [10]. Furthermore, it shows a broader electrochemical window and better mechanical strength. Though it has many advantages, the interfacial contact is poor.

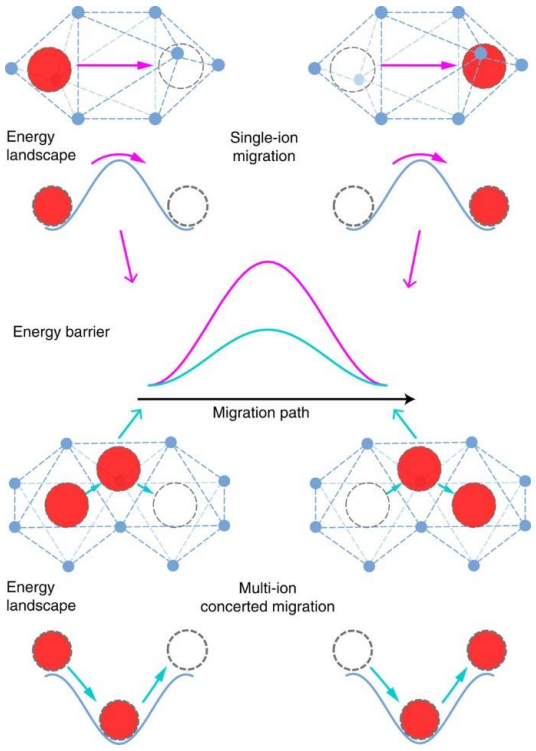

Figure 1.2 Schematic illustration of single-ion migration versus multi-ion concerted migration [11].

We can use the component to classify inorganic solid electrolyte and oxide group is one of which. Lithium lanthanum titanate ($Li_{3x}La_{2/3-x}TiO_3$, LLTO) is one of the conductive ceramic electrolytes with perovskite structure. Due to its remarkable thermal stability over a wide range of voltages and its extremely low electronic conductivity, it has been a popular candidate for solid-state electrolyte. However, there are some limits. First, the presence of grain boundaries causes a significant decrease in ionic conductivity, with values dropping below 10^{-5} S/cm at 298 K. Moreover, when exposed to metallic lithium or graphite anodes, crystalline LLTO is readily to reduction of Ti^{4+} to Ti^{3+}, leading to an increase in electronic conductivity [12]. In the

perovskite structure, Li and La share the A sites and Ti occupies the B sites. A-site vacancies start to form when we increase the La/Li ratio above 1. The maximum conductivity is at x = 0.125 (La/Li = 1.4) from observations. The minimum conductivity sits at x=0.045 [7]. Besides the La/Li ratio, substitutions are another way to reduce bulk conductivity. For example, partially substitute La^{3+} with a larger ionic radius Sr^{2+}. By the substitutions of larger ionic radius metals to the A-site, they increase the lithium concentration by charge compensation and expand the lattice size. A larger lattice size leads to a lower barrier energy [13]. Furthermore, the total conductivity can be attributed to the bulk region and grain boundary. As a result, conductivities differ with different reports because of the distinct grain size and grain boundary composition. Usually, a larger grain size leads to higher conductivity [7].

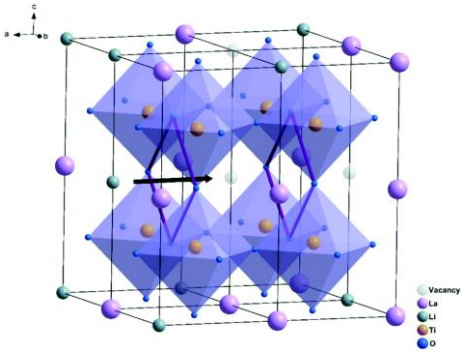

Figure 1.3 Crystal structure of LLTO and the square oxygen window through which the Li ions hop [13].

Another commonly used oxide group electrolyte is lithium lanthanum zirconate ($Li_7La_3Zr_2O_{12}$, LLZO). It is the most promising lithium-stuffed garnet-type solid electrolyte because of its low electronic conductivity of 10^{-8} S/cm at room temperature and a wide

electrochemical operation window of 0–6 V vs. Li^+/Li [13][14]. However, LLZO experiences reduced ionic conductivity when exposed to H_2O and CO_2 at room temperature. Consequently, to prevent this, either the production process should be conducted under an inert atmosphere or additives must be added [15]. LLZO has two polymorphs, a cubic phase (c-LLZO) and a tetragonal phase (t-LLZO). At room temperature, c-LLTO has an ionic conductivity of about 10^{-4} S/cm, and t-LLTO shows an ionic conductivity of 10^{-6} S/cm.

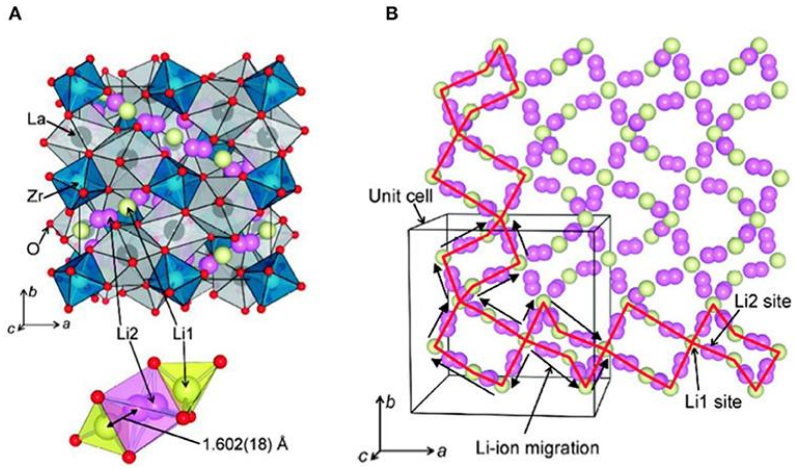

Figure 1.4 (A) LLZO crystal structure and (B) Li-ion conduction channel [16].

Besides the oxide group, the sulfide and phosphates groups are also good ionic conductors. One example of sulfide group electrolytes is a Li_2S/P_2S_5 glass or glass–ceramic. The maximum conductivity of more than 10^{-3} S/cm occurs at 20–30% P_2S_5 because of the degree of crystallization [7][17]. $Li_{1+x}Al_xGe_{2-x}(PO_4)_3$ (LAGP) for phosphate group electrolytes shows the highest conductivities. Another commonly used phosphate electrolyte is $Li_{1+x}Ti_{2-x}Al_x(PO_4)_3$ (LTAP) [7][8].

1.4.2 Solid Polymer Electrolyte

On the other hand, solid polymer electrolyte (SPE) with lithium salt in the matrix is easy to produce, flexible, and has good interfacial contact between electrodes [7][8]. It is a heterogeneous system due to the non-equilibrium of polymer and ionic salt mixture. That is, there are polymer-rich regions and polymer-poor regions [18]. In 1973, Fenton et al. reported a polyethylene oxide (PEO)-alkali metal salts complexation, which in further research proved that the conductivity of PEO could reach 10^{-5} S/cm at about 50 °C [19][20]. Compared with ISE, the conductivity of SPE is lower, the mechanical strength is not ideal, and the thermal and electrochemical properties are more unstable [19].

PEO is an ionic conductive polymer commonly used as SSE because of the strong ether coordination sites. The density of functional group affects the amount of solvated Li-ion and therefore the diffusion of the ion. The polar functional groups (—O—) in PEO can dissolve Li salt, forming PEO- Li salt complexation by Coulombic interaction. In PEO, it is typical for a single Li^+ ion to be coordinated with approximately 4.5 oxygen atoms. The average distance between the Li^+ ion and these oxygen atoms is around 2.55 Å. [21]. The system is generally a dual-ion conductor. That is both lithium ion and its counter anions are movable, although Li^+ is less moveable than the counter anions. The motions of Li ions hopping between oxygen groups are shown in Fig 1.5 and is coupled with Lewis basic sites in the polymer matrix [22]. The transportation can be interchain diffusion, shift, or intrachain diffusion, and the frequent interchain diffusion contributes to the high conductivity [21][22]. In other conductive polymers, the polar functional group could be —B—, —N—, C=O, C≡N, C—S—, and C—(O=S=O) —.

From the mechanism, we can see that the ability of Li^+ to dissociate from the polymer chain will affect the conductivity [8]. The mobility of the polymer chain is another main factor that influences the ion conductivity property. As a result, low-molecular-weight and amorphous PEO shows a better conductivity though the conductivity is still lower than 10^{-4} S/cm at room temperature in general case [22]. Several lithium salts can be used in PEO electrolytes such as $LiClO_4$, $LiPF_6$, $LiBF_4$, $LiSO_3CF_3$ (LiTF), and $LiN(SO_2CF_3)_2$ (LiTFSI). LiTFSI remains the leading candidate among them because of the diffuse charge distribution and resistance to clumping [21][23].

Copolymer electrolytes also have been studied to increase conductivity. In Rakhmawati M. Putri et al.'s work, they added PVA to the PEO electrolyte. PEO/PVA composite has a semicrystalline structure where PEO showed a crystalline structure and PVA showed an amorphous structure. They have successfully increased the ionic conductivity of PVA/PEO/LiOH composite electrolytes to 2.18×10^{-5} S/cm at room temperature [24].

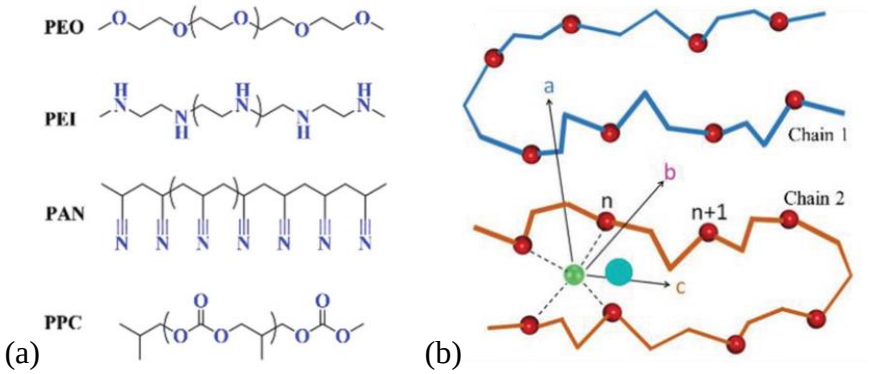

(a) (b)

Figure 1.5 (a) Polar functional groups (blue color) and their representative polymers. (b) Lithium-ion transport mechanisms in polymer chains [22].

1.4.3 Composite Electrolyte

The composite electrolyte could be a polymer with ceramic fillers or a ceramic matrix with polymer. It combines the benefits of both sides of SPE and ISE. The comparison between the traditional electrolytes and SSE is shown in Fig 1.6.

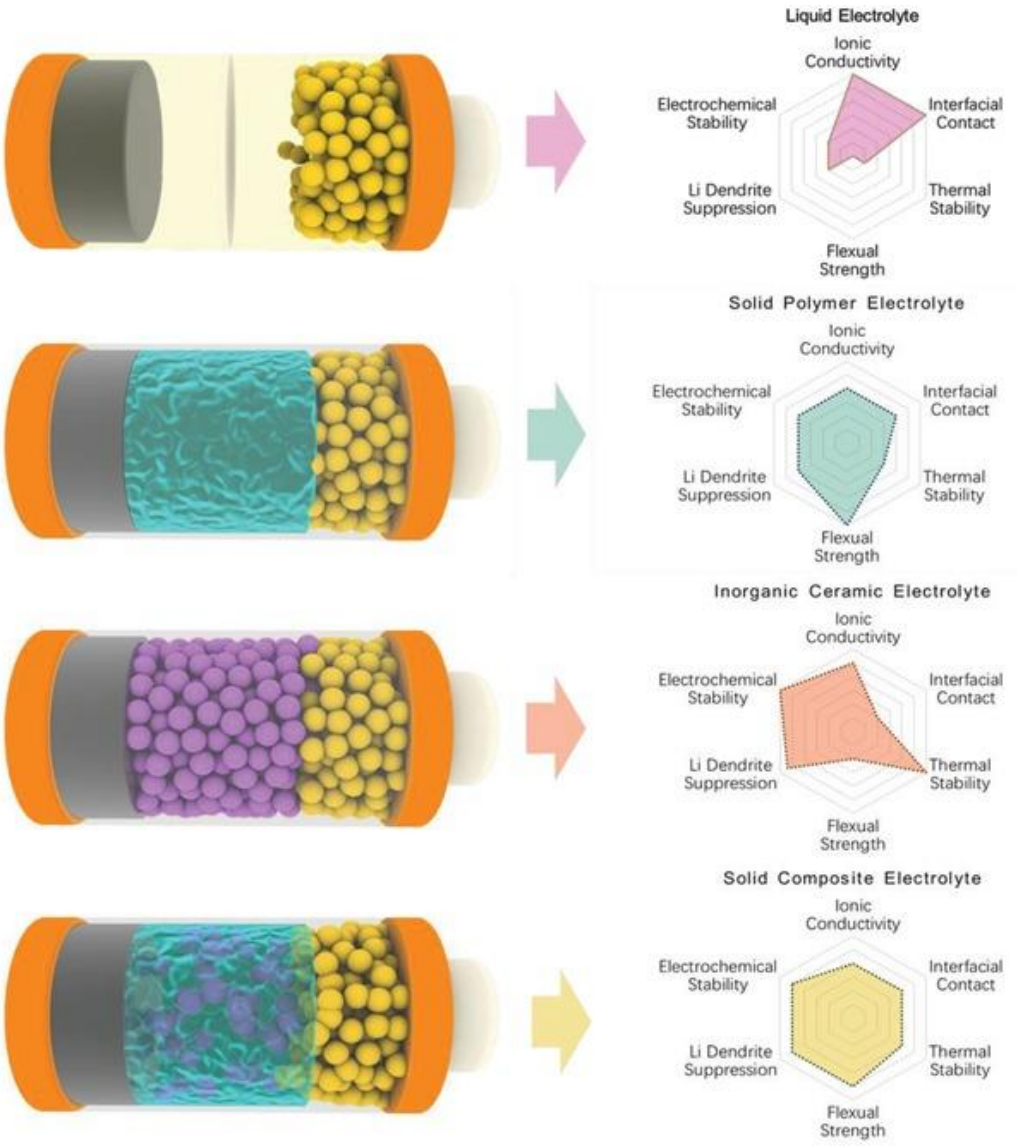

Figure 1.6 The performance comparisons of different electrolytes [25].

In the composite electrolyte, ceramic filler could be either passive or active [26]. Passive filler means the ceramic particles are not ion conductive meaning that there is no Li^+ in the structure. In 1991, Capuano et al. identified that inorganic fillers could improve the phase interfaces' mechanical strength, ionic conductivity, and stability [27]. Kumar and G. Scanlon suggested that polymer and ceramic interfaces act as Li^+ fast transport channels and therefore lead to the enhancement of conductivity, as shown in figure 1.7 [28].

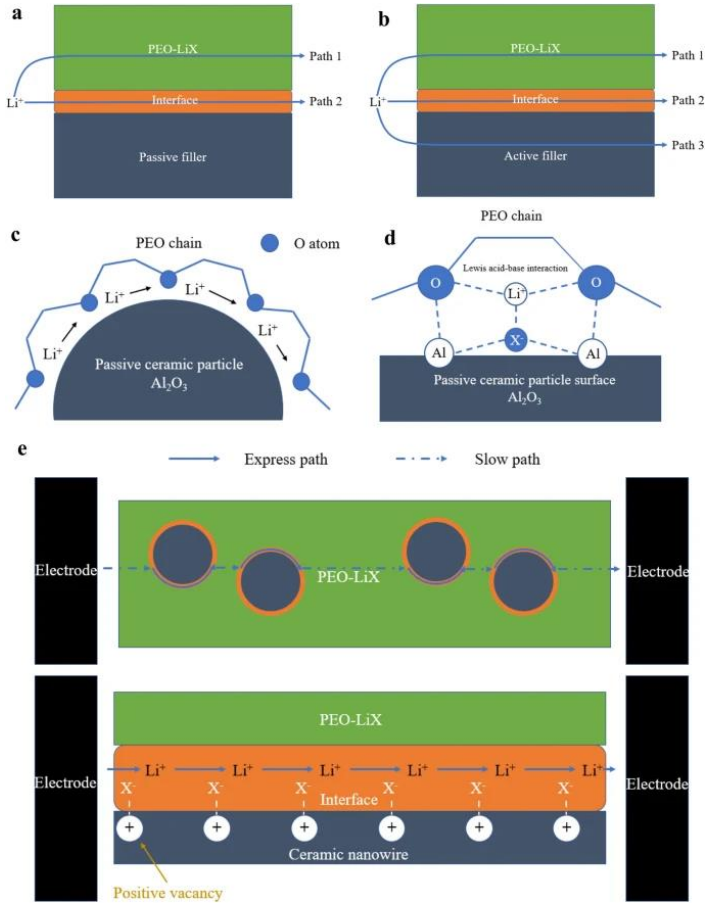

Figure 1.7 (a) Two possible paths of Li+ transport in PEO-passive fillers composite. (b) Three possible paths of Li+ transport in PEO-active fillers composite. (c) Effect of passive fillers

distorting the regularity of PEO. (d) Lewis acid-base interaction on PEO-ceramic interfaces. (e) Long continuous express path of Li+ provided by ceramic nanowires compared with the discontinuous transport path of Li+ provided by ceramic nanoparticles [10].

Another reason for increasing the conductivity is that ceramic particles decrease the crystallinity of PEO [28]. The Lewis acid center of the filler, such as Al atoms on the surface of Al_2O_3, would compete with the cations of lithium salt, forming the complex with Lewis base center on the polymer chain. The filler acts like a cross-linker of the polymer. This would increase the amorphous structures of PEO and suppress the recrystallization process. Moreover, the complex increases the amount of free Li^+. Suppressing the recrystallization process could also explain why the conductivity increases when increasing the temperature [10][29]. Commonly used passive fillers include Al_2O_3, SiO_2, TiO_2, ZnO, and ZrO_2.

Active filler, on the other hand, is a filler containing lithium ions. Commonly used materials include Li_3N, $LiAlO_2$, $Li_{1+x}Al_xGe_{2-x}(PO4)_3$ (LAGP), $Li_{1+x}Al_xTi_{2-x}(PO4)_3$ (LATP), $Li_{3x}La_{2/3-x}TiO_3$ (LLTO), $Li_7La_3Zr_2O_{12}$ (LLZO). These materials can increase the conductivity more than passive filler does because there is one more path for Li^+ transportation. These fillers are more commonly classified based on their structure. They are divided into six categories: NASICON (Na superionic conductor)-type, LISICON (Lithium superionic conductor)-type, Perovskite-type, Garnet-type, Li_3N-type and BPO_4-type [8][10].

The shape of ISEs and filler dispersion present a significant influence on the Li ion conduction in SSEs because it can tune the tortuosity. Tortuosity (τ) is defined as the ratio of

material length to the real length particles traveling in the material, as shown in Fig 1.8. The lower the tortuosity is, the fewer obstacles there are for particles to pass through.

$$\tau = \frac{L_t}{L} (1)$$

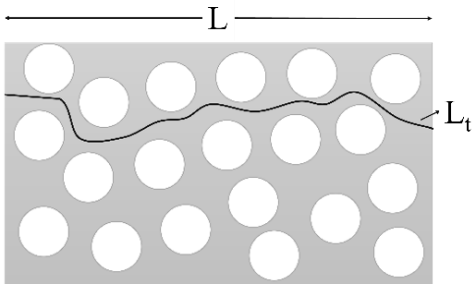

Figure 1.8 Tortuosity of a porous material.

For example, Liu, W. et al have developed aligned inorganic conductive nanowires composite electrolyte as shown in Fig 1.9 (c). The ion conductivity is 6.05×10^{-5} S/cm at 30 °C. Random nanowires in composite electrolytes could supply a more continuous fast pathway for Li ions than isolated nanoparticles. In the case of aligned nanowires, the pathway is generally less tortuous compared to that of random nanowires because there are no crossing junctions present. [30].

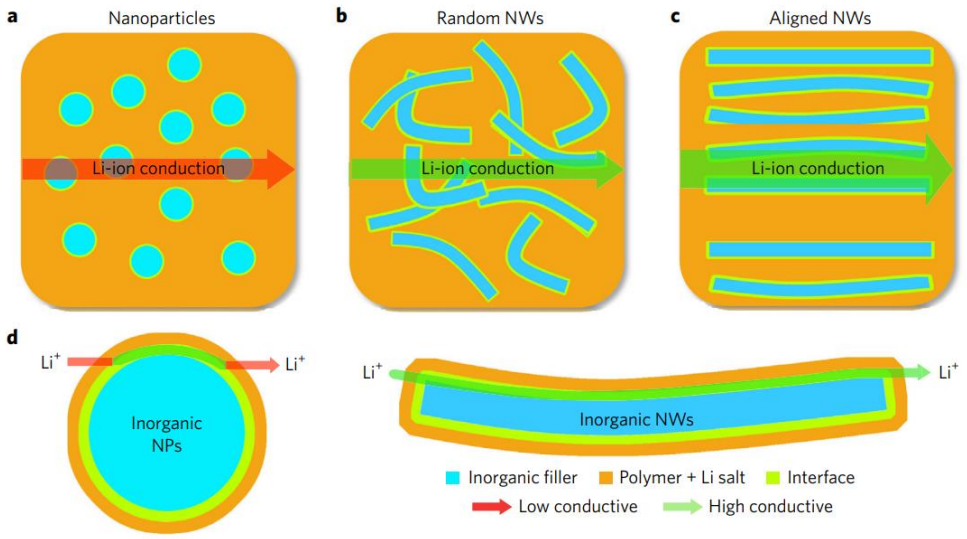

Figure 1.9 The comparison of possible Li-ion conduction pathways. a–c, Li-ion conduction pathways in composite polymer electrolytes with nanoparticles (a), random nanowires (b), and aligned nanowires (c). d, The surface region of inorganic nanoparticles (NPs) and nanowires (NWs) acts as an expressway for Li-ion conduction [30].

Though SSE could reduce the risk of explosion or fire accidents, there are still some challenges to overcome before being widely used in commercial batteries [3]. For example, it shows low coulombic efficiency, low cycle life, high interfacial impedance, and low ionic conductivity. A desired solid-state electrolyte should have high conductivity to transport ions, great electrode/electrolyte interfacial contact to achieve low interfacial impedance, and great mechanical strength to prevent dendrite growth and special processing [8]. However, it couldn't be too hard either, which will lead to poor contact. It should be compatible with the electrode. In the traditional sintering method of fabricating ceramic electrolytes, it made thick samples [3].

The alternative of processing thin film, such as pulsed laser deposition (PLD), radio frequency magnetron sputtering, and atomic layer deposition can achieve a thickness of fewer than 1 μm, but it required either vacuum technology or long-time processing [6].

Here we used the cononsolvency PVA as the template and added LLTO powders and PEO into the framework to make a composite electrolyte. By using an open porous PVA as a template and the LLTO ceramic filler, we expected to increase the mechanical strength, but not lower the conductivity too much. The open porous PVA is made by the cononsolvency effect. It's a phenomenon in that solubility of macromolecule decreases in the mixture of two good solvents. Because the solubility of a macromolecule decreases, it induces phase separation in the solution, forming a polymer-rich region and a solution-rich region. From Fig 1.10 (D) and (E), the gels with 60 wt% DMSO showed the best mechanical performances. The degree of crystallinity increases with the increase of DMSO to 60 wt%. Therefore, the mechanical properties increase. However, when the content of DMSO kept increasing, the degree of crystallinity decreased. On a molecular level, DMSO tends to establish a greater number of hydrogen bonds with water, resulting in the disruption of the hydrogen bond between PVA and water. This promotes the formation of hydrogen bonds between the hydroxyl groups present in PVA chains. As a result, more hydrogen bonds formed between polymer chains and lead to a collapse of the gel matrix in the binary mixture. This was indicated by the porous and fibrous structures in the gel matrix [31].

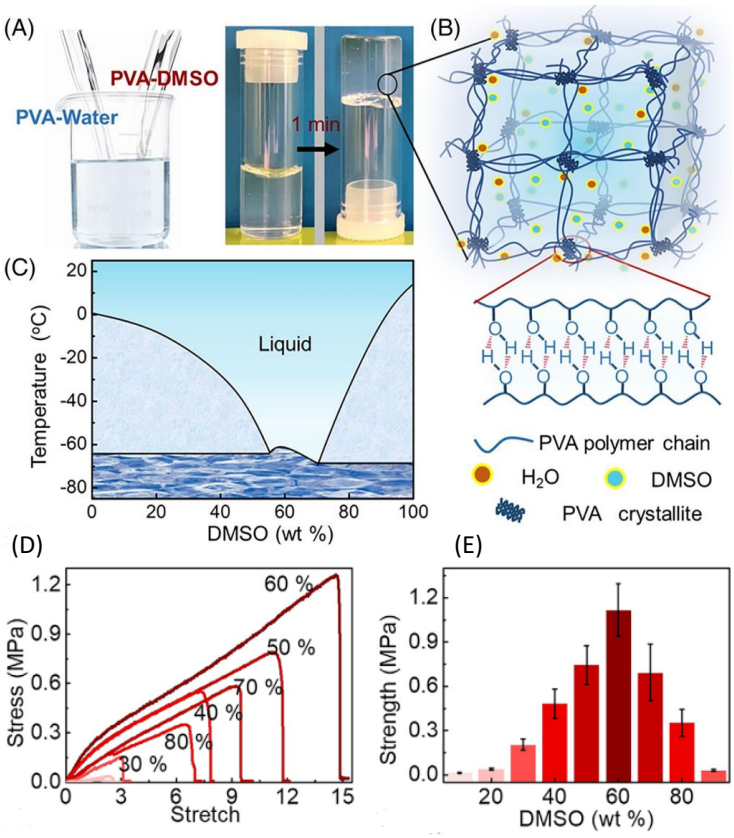

Figure 1.10 (A) Gelation process of the gels: PVA-DMSO and PVA-water solutions both containing 10 wt % PVA were first mixed. The mixture was placed in a −20 °C freezer. Within 1 minute, gelation could be observed when the vial was inverted, and the gel remained at the bottom of the vial. (B) Gelation occurred because of the formation of hydrogen bonds. (C) Phase diagram of the mixture of DMSO and water. (D) Stress-strain curves of gels containing different DMSO content. (E) Strengths of the gels with different DMSO content, from 10 to 90 wt% [31].

Chapter 2 Experimental Section

2.1 Materials and Methods

2.1.1 Materials

Poly (vinyl alcohol) (PVA) (Mw.89000-98000, 99% hydrolyzed), lithium carbonate (≧ 99 %), titanium(IV) oxide (21 nm primary particle, ≧ 99.5 % trace metals), lanthanum(III) nitrate hexahydrate (99.99 % trace metal bases) and dimethyl sulfoxide (DMSO) were purchased from Sigma Aldrich. Lithium bis(trifluoromethylsulfonyl)imide (99 %) was purchased from thermos science. Polyethylene 200 and polyethylene 6000 were purchased from Alfa Aesar. Acetonitrile was purchased from Fisher Chemical.

2.1.2 Preparation of LLTO

Titanium oxide, lithium carbonate, and lanthanum (III) nitrate hexahydrate were mixed with water in stoichiometry molar ratio. Besides, another 20 wt% of lithium carbonate was added to the solution to compensate for the salt evaporation during sintering. Then they were put in the oven for drying. After that, it was sintered to 1200 °C for 6 hours. It was first heated to 200 °C at 6 °C/min and then 1 °C/min to 1200 °C.

2.1.3 Preparation of Composite Electrolyte

To make 5 %, 8 %, and 10 % PVA, a given amount of PVA (Mw 89 000-98 000) was dissolved in water and DMSO separately in a 90 °C water bath. They are termed PVA-DMSO and PVA-water. The PVA-DMSO and PVA-water solutions were mixed weight ratio of 6:4. Then 1 g, 2 g, 4 g, and 8 g LLTO powder was added to 10 g solution and magnetically stirred to make a uniform solution. The mixtures were sandwiched between two glass slides and put into a

−20 °C freezer to facilitate the gelation process. After gelation, the gel sample was soaked in pure water several times to wash out DMSO. Then as-prepared gels were freeze dried by a Labconco FreeZone freeze dryer (termed PVA/LLTO) and soaked in PEO solution under vacuum conditions for three days. The PEO solution was made by dissolving PEO and LiTFSI in acetonitrile with EO: Li^+ ratio of 10:1. The reference sample was made by soaking glass fiber in the PEO solution under vacuum conditions for three days.

Figure 2.1 The structure of sample during freeze dry.

Table 1 Summary of samples with high molecular weight PEO (each section of the name represents the parameter of each cell)

	PVA concentration of the precursor	LLTO concentration in the precursor	EO: Li^+
PVA10/LLTO1/10	10 %	1 g	10:1
PVA10/LLTO2/10	10 %	2 g	10:1
PVA10/LLTO2/13	10 %	2 g	13:1
PVA10/LLTO4/10	10 %	4 g	10:1
PVA10/LLTO4/13	10 %	4 g	13:1
PVA10/LLTO8/10	10 %	8 g	10:1

PVA8/LLTO1/10	8 %	1 g	10:1
PVA8/LLTO2/10	8 %	2 g	10:1
PVA8/LLTO2/13	8 %	2 g	13:1
PVA8/LLTO4/8	8 %	4 g	8:1
PVA8/LLTO4/10	8 %	4 g	10:1
PVA8/LLTO2/13	8 %	4 g	13:1
PVA8/LLTO2/20	8 %	4 g	20:1
PVA8/LLTO8/10	8 %	8 g	10:1
PVA5/LLTO2/10	5 %	2 g	10:1

Table 2 Summary of samples with high molecular weight and low molecular weight PEO with EO: Li^+ ratio of 10:1

	PVA concentration of the precursor	LLTO concentration in the precursor	High molecular weight: low-molecular-weight PEO
PVA8/LLTO4/10	8 %	4 g	1:0
PVA8/LLTO4/10/64	8 %	4 g	6:4
PVA8/LLTO4/10/L	8 %	4 g	0:1

2.2 Characterizations of Material Structure

2.2.1 X-ray diffraction (XRD)

It is a non-destructive method of measuring the component and crystal structure of a material. The incident beam diffracts in the material and forms constructive interference of X-rays in different directions. The diffracted beam satisfies Bragg's law. As a result, every material has its unique peak at different diffraction angles.

$$2dsin\theta = n\lambda \quad (1)$$

where d is the distance between atomic layers in a crystal, θ is the incident angle, n is any integer, and λ is the wavelength of the incident X-ray beam. In this work, XRD was used to confirm the $LiCO_3$, $La(NO_3)_3 \cdot 6H_2O$, and $LiNO_3$ turned into LLTO successfully.

2.2.2 Tensile test

The samples were first cut into dog-bone-shaped specimens with a width of 2 mm for regular tensile tests. The thickness of the specimens was gauged with a caliper. The force-displacement data were obtained by using a Cellscale Univert mechanical tester with a 50 N loading cell installed. By division of an initial gauge cross-section area and an initial clamp distance, the stress-strain curves were obtained.

2.2.3 Electrochemical Impedance Spectroscopy (EIS)

The composite films were put between two stainless steel electrodes with a clip to test for EIS at room temperature. First, the conductivity was measured by the electrochemical AC impedance spectroscopy (IMP) method with frequency ranges from 10 to 10^6 Hz and a voltage of

0.5 V. The intercept of the x-axis is the resistance of the sample. Accordingly, the ionic conductivity of hydrogels was calculated with Eq (2).

$$\sigma = \frac{L}{RA} \quad (2)$$

where L is the distance between the two probes, R represents the electrical resistance, and A represents the cross-sectional area of the sample.

EIS is a rapid and non-destructive method commonly used to obtain ion conductivity. By applying a small sinusoidal voltage perturbation through the sample, we can obtain the current response, which is dependent on the frequency. Then the impedance can be calculated. Impedance (Z) in alternating current (AC) is equivalent to the resistance in direct current (DC). That is, it is a measure of the opposition to electrical flow. However, unlike DC, there are effects of the generation of voltages (inductance) and the storage of electrical charge (capacitance) in AC circuits. The inductance is generated by the magnetic fields and the capacitance is induced by voltages between conductors. Impedance is a complex number, which contains both a magnitude characteristic and a phase angle. It is often expressed in Cartesian form Eq 3.

$$Z = Z_{re} + jZ_{im} \quad (3)$$

where the real part of the impedance is the resistance Z_{re}, the imaginary part is the reactance Z_{im}, and j is the imaginary unit.

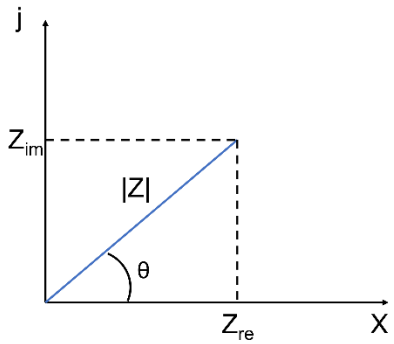

Figure 2.2 A vector illustration of impedance in a Nyquist plot

2.2.4 SEM

To characterize the micro- and nano- structures of the samples, the image was carried out by using a ZEISS Supra 40VP SEM. All freeze-dried samples before being immersed in PEO solution were cut to expose the inside and sputtered with gold.

2.2.5 Linear Sweep Voltammetry (LSV)

The LSV was conducted with a scan rate of 0.1 mV/sec between 0 to 4 V to study the electrochemical window of the composite electrolyte. The electrolyte samples were put between two stainless steel electrodes in the coin cell.

2.3 Results and Discussion

2.3.1 Characterizations of LLTO and PVA Template

From the literature, a well-crystallized LLTO phase could be obtained by sintering the precursor at 900 °C for 6 h. The XRD pattern also demonstrates the presence of La, Li, and vacancies ordering arrangement along the c-axis (indicated by arrows), Fig 2.3. However, there

are $La_2Ti_2O_7$ and $LiLaO_2$ impurities in the samples. With the increasing sintering temperature, impure phase $La_2Ti_2O_7$ decreases, the grain size increases, and the conductivity increases [32].

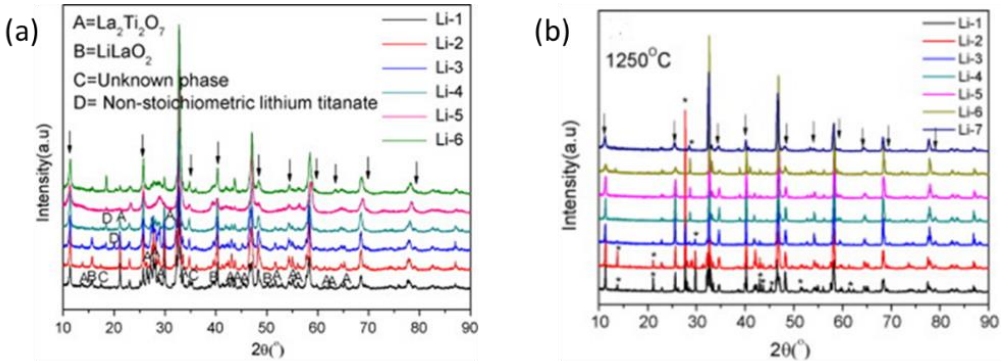

Figure 2.3 (a) XRD patterns of the LLTO powders with different lithium contents prepared by sol-gel method at 900 °C. (b) XRD patterns of the LLTO powders with different lithium contents prepared by sol-gel method at 1250 °C (c) Real compositions in the LLTO powders calcined at 900 °C and pellets sintered at 1250 °C [32].

In this work, the XRD spectrum of LLTO sintered at 60 °C for 6 hours is shown in Fig 2.4 (a) and matches the standard PDF card JCPDS No. 870935 in Fig 2.4 (b). These peaks correspond with the peak of the (110) facet (32°), (112) facet (40°), (200) facet (47°), (201) facet (48°), and (212) facet (58°) of the LLTO target. It showed sharp diffraction peaks in the XRD pattern, which indicated the crystalline structure of sintered LLTO. Also, peaks at 26°, 35°, 40°, and 47°, etc. indicated the presence of La, Li, and vacancies along the c-axis. There are some minor peaks (orange dash circles) that indicate a small amount of $La_2Ti_2O_7$ and $LiLaO_2$ impurities of the synthesized $Li_{0.33}La_{0.57}TiO_3$.

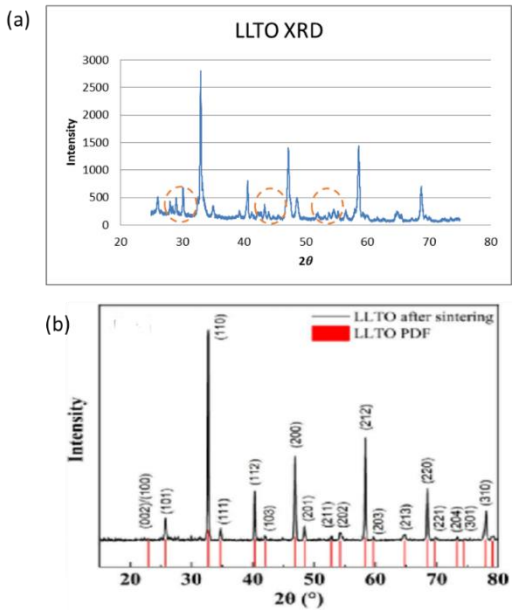

Figure 2.4 (a) XRD characterization of sintered LLTO ceramic powder of my work. (b) XRD data of the LLTO powders compared with standard PDF card JCPDS No.870935 of Pengyu Xu et al. 's work [33].

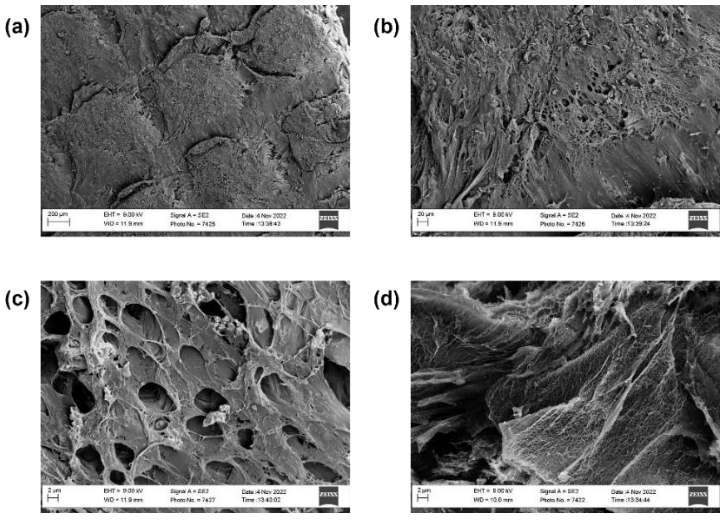

Figure 2.5 SEM image of PVA/LLTO sample (PVA8/LLTO8 as an example). (a~c) surface structure in a different scale and (d) cross section.

2.3.2 Conductivity

The EIS plot was used to obtain the conductivities. It includes a real part and an imaginary part. For polymer electrolytes, the system can be represented by standard electrical components, the resistor, and the capacitor. The resistive characteristic is attributed to the real part and the capacitive property to the imaginary part of the Nyquist plot. From Fig 2.6, we can see a semicircle and a tilted spike, which is the typical Nyquist plot for polymer electrolytes. The behavior is similar to the Randle circuit (RC), an equivalent circuit often used to describe the electrical behavior of solid polymer electrolytes, (Fig 2.7 (a)). The semicircle in the high-frequency range indicates the bulk impedance of the polymer electrolyte, and the low-frequency inclined tail is related to the interfacial impedance or ion diffusion.

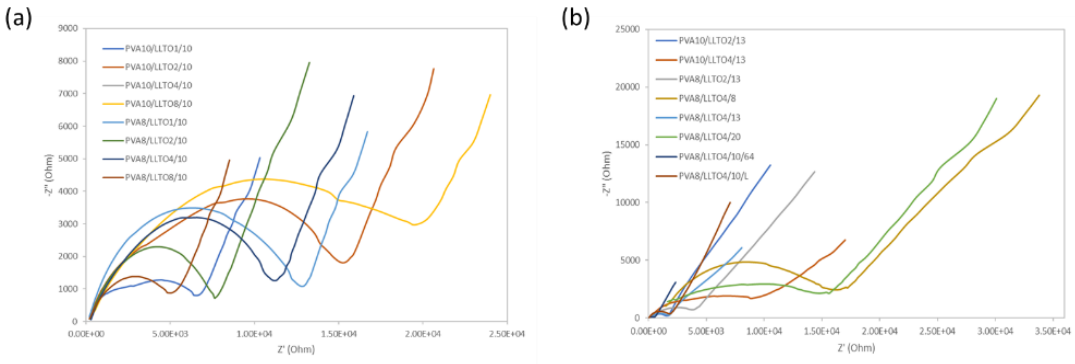

Figure 2.6 (a, b) Nyquist plot of the samples.

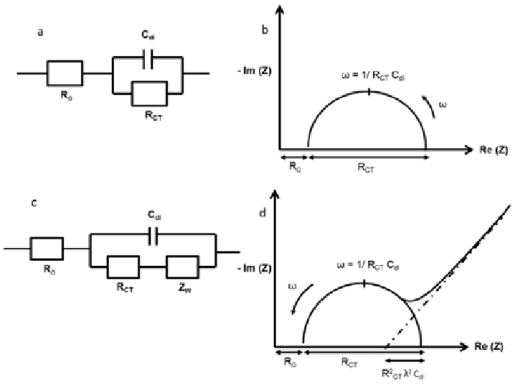

Figure 2.7 (a) Representation of Randles circuit, (b) its characteristic Nyquist plot, (c) Randles circuit with Warburg element, and (d) its characteristic Nyquist plot [37].

With the same concentration of PVA and the same ratio of EO: Li^+, the more ceramic, the higher conductivity is. It showed the maximum conductivity with PVA10/LLTO4/10 (1.32×10^{-4} S/cm) and PVA8/LLTO2/10 (1.33×10^{-4} S/cm), Fig 2.8. This may be caused by the agglomeration of ceramic powder when the concentration of the ceramic is high. Furthermore, with more PVA in the sample, there is less porous space for ceramic powder. Aggregation happens more easily. As a result, the maximum conductivity happened in 2 g when the concentration of PVA precursor is 10 %. We can confirm this by the SEM image. From Fig 2.9 (a), we see the structure of pure PVA. In Fig 2.9 (b) and (c), we can assume that the white particles are LLTO powders, and there were ceramic particles in both the cross section and surface. However, in the 8 g sample, the LLTO particles only appeared on the surface. The ceramic particles aggregated to the surface.

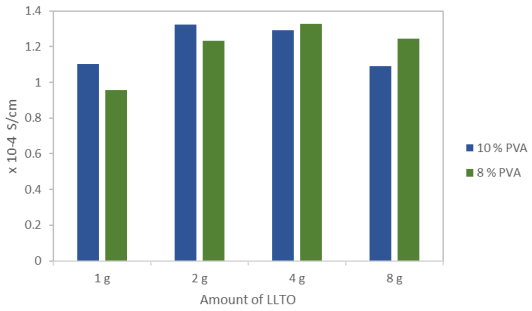

Figure 2.8 Conductivities of 10 % PVA, EO: Li^+ 10:1 and 8 % PVA, EO: Li^+ 10:1 with different amounts of LLTO in the precursor.

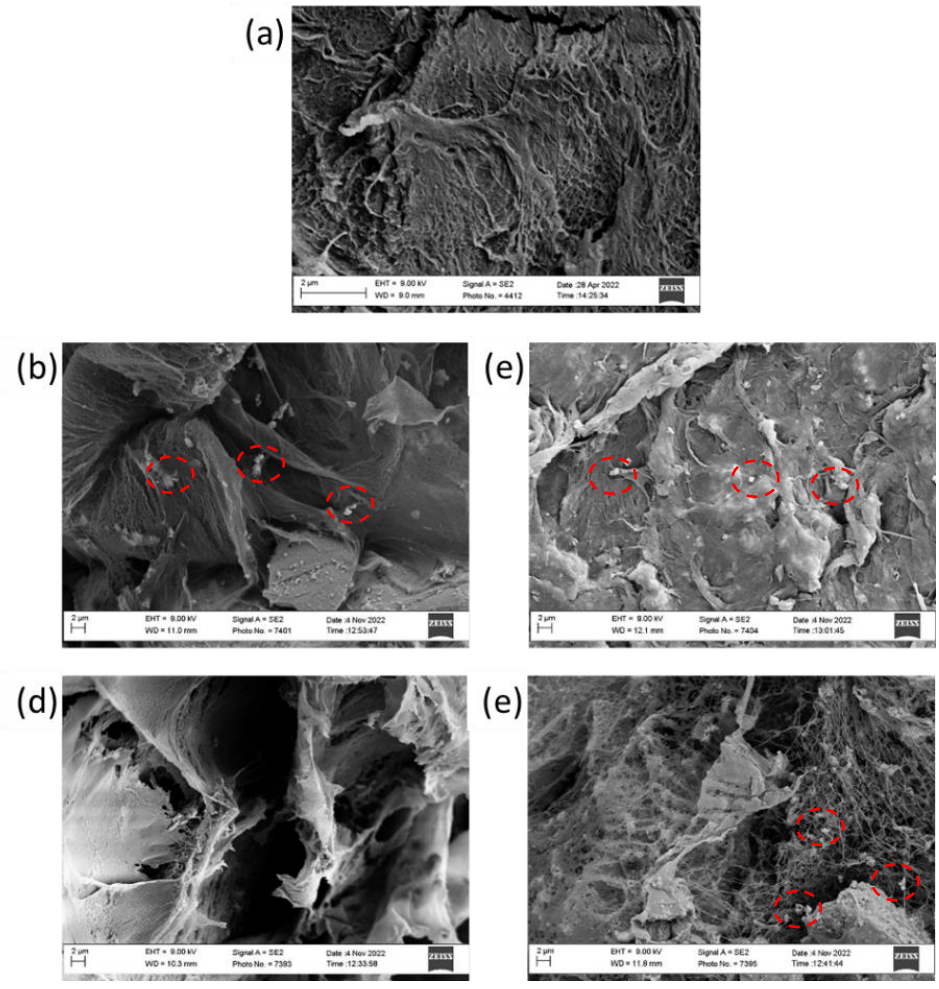

Figure 2.9 SEM image of (a) pure PVA (b) cross section of PVA10/LLTO4 (c) surface of PVA10/LLTO4 (d) cross section of PVA10/LLTO8 and (e) surface of PVA10/LLTO8. The red dash circle indicates the ceramic particle.

As mentioned, the mobility of the polymer chain also affects ion conductivity. From Fig 2.10 (a), low-molecular-weight PEO shows the highest conductivity of 2.03×10^{-4} S/cm. Besides the concentration of PVA and molecular weight of PEO, the EO: Li^+ ratio is another factor that affects ion conductivity. In Fig 2.10 (b), the EO: Li^+ ratio of 8:1 shows the lowest conductivity. The results may be caused by the anion coordinating the Li cation in the system. The anion coordination effect is weaker in the lower salt concentration case. However, in high anion concentration systems, the effect of clusters becomes significant, and a new ensemble of Li^+-oxygen coordination forms [34].

With other PVA/PEO/LiOH composite electrolytes in the literature, the conductivity is 2.18×10^{-5} S/cm at room temperature [24]. The PEO/LLTO-nanowires composite electrolyte showed a conductivity of 5.53×10^{-5} S/cm [35]. We have improved the ionic conductivities with the PVA, PEO, and LLTO composite electrolytes.

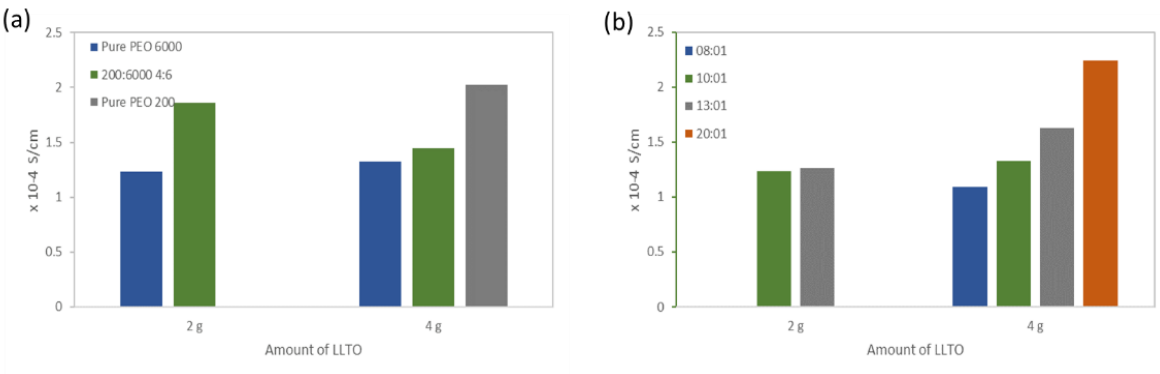

Figure 2.10 (a) Conductivities of 8 % PVA with different molecular weight concentrations of PEO (b) Conductivities of 8 % PVA-2 g LLTO (PVA8/LLTO2) and 8 %-4 g LLTO (PVA8/LLTO4) samples with different EO: Li^+ ratios.

2.3.3 Strength

With more PVA templates in the sample, it showed a higher mechanical strength. With 10 % and 8 % PVA in the precursor, Young's modulus can reach around 120 MPa and 15 MPa respectively. With 5 % PVA in the precursor, Young's modulus dropped to 6 MPa. For the 5 % PVA sample, the PVA/LLTO gel sample is even too weak to wash out DMSO. With more LLTO concentration, Young's modulus were higher because of its cross-link function. Moreover, PVA10/LLTO4/10 showed the tensile strength of 9 MPa, and PVA8/LLTO4/10 showed the tensile strength of 1.2 MPa. Compared with the reference sample, though it showed a high conductivity of about $2x10^{-4}$ S/cm, the mechanical strength is very low (Fig 2.11 (b)). Hence, using PVA as the template can increase mechanical strength.

From previous work, the tensile strength of the PEO/polyaryl polymethylene isocyanate (PAPI) membrane with 0.4 ml PAPI is 10.0 MPa and Young's modulus is 49.4 MPa [36]. The PEO/PVDF/LiClO4/SN sample with Young's modulus of 4.2 MPa, the maximum stress of 3.37 MPa [37]. Compared with these electrolytes, our samples showed a better property.

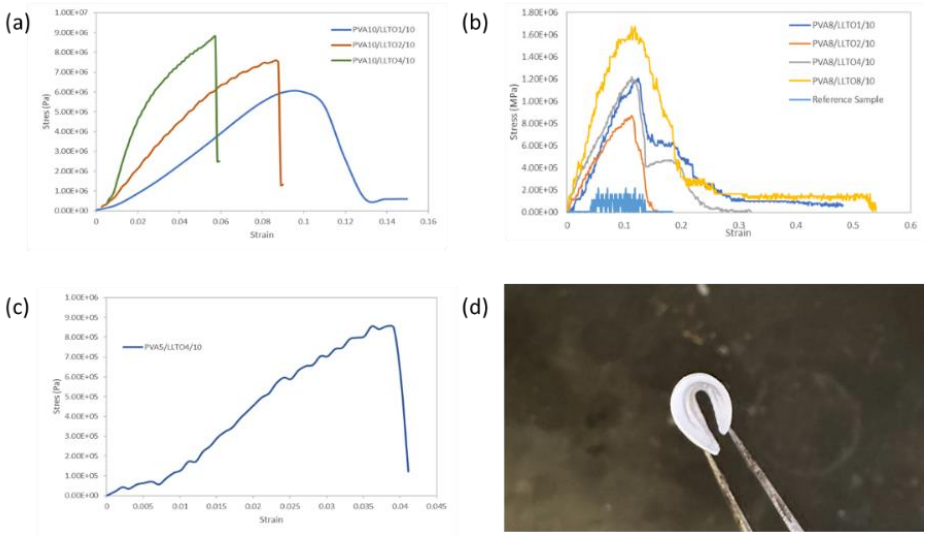

Figure 2.11 Stress-strain curve of (a) 10 % PVA (b) 8 % PVA (c) 5 % PVA samples with the ratio EO: Li^+ of 10:1 and different concentrations of LLTO in the precursor.

2.3.4 Linear Sweep Voltammetry (LSV)

The operating voltage range of the battery is affected by the electrochemical window. From Fig 2.12, the oxidative current of both composite and reference samples was close to zero until the voltage reached about 2.8 V. Since both the electrodes are stainless steels, there are two explanations. First, the reference voltage shifted so that the electrochemical window we measured is lower than the usual oxidation voltage of 4 V. Seconds, both samples are unstable in

the condition. To further determine the problem, we would want to assemble the coin cell with Li foil | composite electrolyte | stainless steel in the glove box and test the LSV test again. In the meantime, we can try to add glutaraldehyde as the crosslinker of PVA to increase the stability.

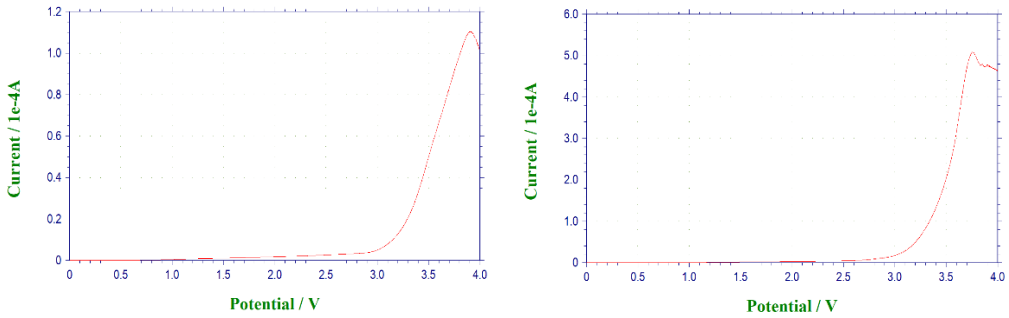

Figure 2.12 The LSV curve for (a) composite electrolyte and (b) pure PEO-LiTFSI reference sample with glass fiber as the separator.

Chapter 3: Conclusion and Outlook

Solid-state electrolyte research has greatly increased due to the growing pursuit of electric vehicles and portable electronics. In this study, we made a potential composite electrolyte with high ionic conductivity without compensating the mechanical properties. A range of conductivities above 10^{-4} S/cm was successfully obtained with Young's modulus as high as 40 MPa and 120 MPa. Considering of both mechanical strength and conductivity, PVA10/LLTO2, PVA10/LLTO4, and PVA8/LLTO4 would be the best choice. Further work would include doing the CV test and cycling test to make sure the electrolyte can reach a good performance in the battery. The optimized concentration of each component is needed to be confirmed. With the research so far, I estimate it would be 10 % PVA and 2 g LLTO powder of precursor pairing

with EO: Li^+ 20:1. Other parameter like the particle size of the ceramic powder could also influence conductivities and mechanical properties. We can determine the particle size more precisely with the help of a milling machine. With smaller particles, the particles would disperse more uniformly and the alignment with the PVA template would be better. Besides, the conductivity in grain boundary is low, so we would also want to reduce grain boundaries. As a result, we would like to make the LLTO particles connect in the PVA framework. First possible method would be adjusting the process. That is, we sinter porous LLTO thin film first. Then immerse it into the cononsolvency PVA solution and form gel. Follow with freeze dry and PEO solution immersion. Another possible solution is that make PVA chain and LLTO particle charged oppositely. With the help of charge attraction, LLTO powder is assumed to align better on the PVA framework and connect each particles. After the immersion of PEO solution, co-cold sintering of all components, electrodes and electrolyte, is conducted to densify each component and have a better contact between each layer [38].

References

[1] M. S. Whittingham, "Electrical Energy Storage and Intercalation Chemistry," *Science (1979)*, vol. 192, no. 4244, pp. 1126–1127, Jun. 1976, doi: 10.1126/science.192.4244.1126.

[2] N. Nitta, F. Wu, J. T. Lee, and G. Yushin, "Li-ion battery materials: present and future," *Materials Today*, vol. 18, no. 5, pp. 252–264, 2015, doi: https://doi.org/10.1016/j.mattod.2014.10.040.

[3] Y. Chen *et al.*, "A review of lithium-ion battery safety concerns: The issues, strategies, and testing standards," *Journal of Energy Chemistry*, vol. 59, pp. 83–99, 2021, doi: https://doi.org/10.1016/j.jechem.2020.10.017.

[4] J. B. Goodenough and K. S. Park, "The Li-ion rechargeable battery: A perspective," *J Am Chem Soc*, vol. 135, no. 4, pp. 1167–1176, Jan. 2013, doi: 10.1021/JA3091438/ASSET/IMAGES/MEDIUM/JA-2012-091438_0009.GIF.

[5] K. Xu, "Nonaqueous liquid electrolytes for lithium-based rechargeable batteries," *Chem Rev*, vol. 104, no. 10, pp. 4303–4417, Oct. 2004, doi: 10.1021/CR030203G/ASSET/CR030203G.FP.PNG_V03.

[6] Z. Zheng, S. Song, and Y. Wang, "Sol-gel-processed amorphous lithium ion electrolyte thin films: Structural evolution, theoretical considerations, and ion transport processes," *Solid State Ion*, vol. 287, pp. 60–70, Apr. 2016, doi: 10.1016/J.SSI.2016.02.006.

[7] J. W. Fergus, “Ceramic and polymeric solid electrolytes for lithium-ion batteries,” *J Power Sources*, vol. 195, no. 15, pp. 4554–4569, Aug. 2010, doi: 10.1016/J.JPOWSOUR.2010.01.076.

[8] P. Yao *et al.*, “Review on Polymer-Based Composite Electrolytes for Lithium Batteries,” *Front Chem*, vol. 7, p. 522, Aug. 2019, doi: 10.3389/FCHEM.2019.00522/BIBTEX.

[9] E. Quartarone and P. Mustarelli, “Review—Emerging Trends in the Design of Electrolytes for Lithium and Post-Lithium Batteries,” *J Electrochem Soc*, vol. 167, no. 5, p. 050508, Jan. 2020, doi: 10.1149/1945-7111/AB63C4.

[10] J. Feng, L. Wang, Y. Chen, P. Wang, H. Zhang, and X. He, “PEO based polymer-ceramic hybrid solid electrolytes: a review,” *Nano Converg*, vol. 8, no. 2, 2021, doi: 10.1186/s40580-020-00252-5.

[11] X. He, Y. Zhu, and Y. Mo, “Origin of fast ion diffusion in super-ionic conductors,” *Nature Communications 2017 8:1*, vol. 8, no. 1, pp. 1–7, Jun. 2017, doi: 10.1038/ncomms15893.

[12] Y. Sun, P. Guan, Y. Liu, H. Xu, S. Li, and D. Chu, “Recent Progress in Lithium Lanthanum Titanate Electrolyte towards All Solid-State Lithium Ion Secondary Battery,” *https://doi.org/10.1080/10408436.2018.1485551*, vol. 44, no. 4, pp. 265–282, Jul. 2018, doi: 10.1080/10408436.2018.1485551.

[13] A. Jonderian and E. McCalla, “The role of metal substitutions in the development of Li batteries, part II: solid electrolytes,” *Mater Adv*, vol. 2, no. 9, pp. 2846–2875, May 2021, doi: 10.1039/D1MA00082A.

[14] K. v. Kravchyk, D. T. Karabay, and M. v. Kovalenko, “On the feasibility of all-solid-state batteries with LLZO as a single electrolyte,” *Scientific Reports 2022 12:1*, vol. 12, no. 1, pp. 1–10, Jan. 2022, doi: 10.1038/s41598-022-05141-x.

[15] W. G. Suci, H. K. Aliwarga, Y. R. Azinuddin, R. B. Setyawati, K. N. R. Stulasti, and A. Purwanto, “Review of various sulfide electrolyte types for solid-state lithium-ion batteries,” *Open Engineering*, vol. 12, no. 1, pp. 409–423, Jan. 2022, doi: 10.1515/ENG-2022-0043/ASSET/GRAPHIC/J_ENG-2022-0043_FIG_006.JPG.

[16] A. Kim, S. Woo, M. Kang, H. Park, and B. Kang, “Research Progresses of Garnet-Type Solid Electrolytes for Developing All-Solid-State Li Batteries,” *Front Chem*, vol. 8, p. 468, Jun. 2020, doi: 10.3389/FCHEM.2020.00468/BIBTEX.

[17] J. Trevey, J. S. Jang, Y. S. Jung, C. R. Stoldt, and S.-H. Lee, “Glass–ceramic Li2S–P2S5 electrolytes prepared by a single step ball billing process and their application for all-solid-state lithium–ion batteries,” *Electrochem commun*, vol. 11, no. 9, pp. 1830–1833, 2009, Accessed: Dec. 26, 2022. [Online]. Available: https://www.academia.edu/11815852/Glass_ceramic_Li2S_P2S5_electrolytes_prepared_by_a_single_step_ball_billing_process_and_their_application_for_all_solid_state_lithium_ion_batteries

[18] S. R. Bt. Abdul Karim, C. H. A. N. Chan, and L. H. A. R. Sim, “Impedance Spectroscopy: a Practical Guide to Evaluate Parameters of a Nyquist Plot for Solid Polymer Electrolyte Applications,” *Functional Polymeric Composites*, pp. 97–128, Nov. 2017, doi: 10.1201/9781315207452-5.

[19] D. E. Fenton, J. M. Parker, and P. V. Wright, “Complexes of alkali metal ions with poly(ethylene oxide),” *Polymer (Guildf)*, vol. 14, p. 589, 1973.

[20] G. C. Farrington and J. L. Briant, “Fast Ionic Transport in Solids,” *Science (1979)*, vol. 204, no. 4400, pp. 1371–1379, Jun. 1979, doi: 10.1126/science.204.4400.1371.

[21] D. J. Brooks, B. v Merinov, W. A. I. I. I. Goddard, B. Kozinsky, and J. Mailoa, “Atomistic Description of Ionic Diffusion in PEO–LiTFSI: Effect of Temperature, Molecular Weight, and Ionic Concentration,” *Macromolecules*, vol. 51, no. 21, pp. 8987–8995, Nov. 2018, doi: 10.1021/acs.macromol.8b01753.

[22] Y. Zhao *et al.*, “Solid Polymer Electrolytes with High Conductivity and Transference Number of Li Ions for Li-Based Rechargeable Batteries,” *Advanced Science*, vol. 8, no. 7. John Wiley and Sons Inc, Apr. 01, 2021. doi: 10.1002/advs.202003675.

[23] Z. Xue, D. He, and X. Xie, “Poly(ethylene oxide)-based electrolytes for lithium-ion batteries,” *J Mater Chem A Mater*, vol. 3, no. 38, pp. 19218–19253, Sep. 2015, doi: 10.1039/C5TA03471J.

[24] R. M. Putri, O. Floweri, T. R. Mayangsari, and A. H. Aimon, “Preliminary study of Electrochemical Properties of Polyethylene Oxide (PEO) and Polyvinyl Alcohol (PVA) composites as material for solid polymer electrolyte,” 2020, Accessed: Dec. 26, 2022. [Online]. Available: www.sciencedirect.com

[25] D. E. Fenton, J. M. Parker, and P. v. Wright, “Complexes of alkali metal ions with poly(ethylene oxide),” *Polymer (Guildf)*, vol. 14, no. 11, p. 589, 1973, doi: 10.1016/0032-3861(73)90146-8.

[26] J. Feng, L. Wang, Y. Chen, P. Wang, H. Zhang, and X. He, "PEO based polymer-ceramic hybrid solid electrolytes: a review," *Nano Converg*, vol. 8, no. 1, p. 2, 2021, doi: 10.1186/s40580-020-00252-5.

[27] F. Capuano, F. Croce, and B. Scrosati, "Composite Polymer Electrolytes," *J Electrochem Soc*, vol. 138, no. 7, p. 1918, Jul. 1991, doi: 10.1149/1.2085900.

[28] B. Kumar and L. G. Scanlon, "Polymer-ceramic composite electrolytes," *J Power Sources*, vol. 52, no. 2, pp. 261–268, 1994, doi: https://doi.org/10.1016/0378-7753(94)02147-3.

[29] W. Wieczorek, Z. Florjanczyk, and J. R. Stevens, "Composite polyether based solid electrolytes," *Electrochim Acta*, vol. 40, no. 13–14, pp. 2251–2258, Oct. 1995, doi: 10.1016/0013-4686(95)00172-B.

[30] W. Liu *et al.*, "Enhancing ionic conductivity in composite polymer electrolytes with well-aligned ceramic nanowires," *Nature Energy 2017 2:5*, vol. 2, no. 5, pp. 1–7, Apr. 2017, doi: 10.1038/nenergy.2017.35.

[31] S. Wu *et al.*, "Rapid and scalable fabrication of ultra-stretchable, anti-freezing conductive gels by cononsolvency effect," *EcoMat*, vol. 3, no. 2, p. e12085, Apr. 2021, doi: 10.1002/EOM2.12085.

[32] H. Geng, J. Lan, A. Mei, Y. Lin, and C. W. Nan, "Effect of sintering temperature on microstructure and transport properties of Li3xLa2/3−xTiO3 with different lithium contents," *Electrochim Acta*, vol. 56, no. 9, pp. 3406–3414, Mar. 2011, doi: 10.1016/J.ELECTACTA.2010.06.031.

[33] P. Xu *et al.*, “Origin of High Interfacial Resistances in Solid-State Batteries: Interdiffusion and Amorphous Film Formation in Li0.33La0.57TiO3/LiMn2O4 Half Cells,” *ChemElectroChem*, vol. 6, no. 17, pp. 4576–4585, Sep. 2019, doi: 10.1002/CELC.201901068.

[34] N. Molinari, J. P. Mailoa, and B. Kozinsky, “Effect of Salt Concentration on Ion Clustering and Transport in Polymer Solid Electrolytes: A Molecular Dynamics Study of PEO-LiTFSI,” *Chemistry of Materials*, vol. 30, no. 18, pp. 6298–6306, Sep. 2018, doi: 10.1021/ACS.CHEMMATER.8B01955/SUPPL_FILE/CM8B01955_SI_001.PDF.

[35] L. Zhu, P. Zhu, Q. Fang, M. Jing, X. Shen, and L. Yang, “A novel solid PEO/LLTO-nanowires polymer composite electrolyte for solid-state lithium-ion battery,” *Electrochim Acta*, vol. 292, pp. 718–726, Dec. 2018, doi: 10.1016/J.ELECTACTA.2018.10.005.

[36] C. Xin *et al.*, “A Cross-Linked Poly(Ethylene Oxide)-Based Electrolyte for All-Solid-State Lithium Metal Batteries With Long Cycling Stability,” *Front Mater*, vol. 9, p. 211, Apr. 2022, doi: 10.3389/FMATS.2022.864478/BIBTEX.

[37] H. Wang *et al.*, “Mechanical property-reinforced PEO/PVDF/LiClO4/SN blend all solid polymer electrolyte for lithium ion batteries,” *Journal of Electroanalytical Chemistry*, vol. 869, p. 114156, Jul. 2020, doi: 10.1016/J.JELECHEM.2020.114156.

[38] J.-H. Seo *et al.*, “Cold sintering, enabling a route to co-sinter an all-solid-state lithium-ion battery,” *Jpn J Appl Phys*, vol. 60, Feb. 2021, doi: 10.35848/1347-4065/abdd4c.